

Material design of elastic structures using Voronoi cells

J.M. Podestá¹, C. Méndez², S. Toro¹, A.E. Huespe^{1,3*}, J. Oliver^{3,4}

¹CIMEC-UNL-CONICET, Predio Conicet Dr Alberto Cassano, CP 3000 Santa Fe, Argentina

²CIMNE-Latinoamérica, Iturraspe 785, CP 3000, Santa Fe, Argentina

³Centre Internacional de Metodes Numerics en Enyinyeria (CIMNE), Campus Nord UPC.

⁴E.T.S dEnginyers de Camins, Canals i Ports, Technical University of Catalonia (Barcelona Tech)
Campus Nord UPC, Mòdul C-1, c/ Jordi Girona 1-3, 08034, Barcelona, Spain

Keywords: inverse material design; two-scale material design; Free Material Optimization (FMO); micro-architecture topology optimization; Topology Optimization Problem (TOP)

Abstract

New tools for the design of metamaterials with periodic micro-architectures are presented.

Initially, a two-scale material design approach is adopted. At the structure scale, the material effective properties and their spatial distribution are obtained through a Free Material Optimization (FMO) technique. At the micro-structure scale, the material micro-architecture is designed by appealing to a Topology Optimization Problem (TOP). The TOP is based on the topological derivative and the level set function.

The new proposed tools are used to facilitate the search of the optimal micro-architecture configuration. They consist of the following:

- i)* a procedure to choose an adequate shape of the unit-cell domain where the TOP is formulated. Shapes of Voronoi-cells associated with Bravais lattices are adopted.
- ii)* a procedure to choose an initial material distribution within the Voronoi cell being utilized as the initial configuration for the iterative topology optimization algorithm.

*Corresponding author. E-mail address: ahuespe@intec.unl.edu.ar (A.E. Huespe).

Symbols for elasticity tensors

- \mathbf{C} : Generic effective fourth order symmetric elasticity tensor expressed in Cartesian coordinates.
- \mathbf{C}_N : Generic effective elasticity tensor expressed in normal form (see sub-Section 2.2.2 and Appendix B).
- $\hat{\mathbf{C}}$: Effective elasticity tensor solution of the FMO problems expressed in Cartesian coordinates (Section 3).
- $\hat{\mathbf{C}}_N$: Effective elasticity tensor solution of the FMO problems expressed in normal form (sub-Section 3.3).
- \mathbf{C}^* : Effective elasticity tensor being the average of $\hat{\mathbf{C}}_N$ in a given body sector (sub-Section 3.3).
- \mathbf{C}^h : Homogenized elasticity tensor evaluated with a micro-cell (using a computational homogenization technique, Section 4) expressed in Cartesian coordinates.
- \mathbf{C}_N^h : Tensor \mathbf{C}^h expressed in normal form.
- \mathbf{C}_{db}^h : Homogenized tensor constituting the database (sub-Section 5.2) expressed in normal form.
- \mathbf{C}_μ : Micro-scale elasticity tensor (Section 4).

1 Introduction

In the early 1990's, after the seminal papers of Bendsøe and coauthors ([1]–[2]), the contribution of Ringertz [3] and the book of Bendsøe [4], the Free Material Optimization (FMO) methodology has become a well-established technique in the mechanical structural optimization community. This methodology seeks, in a given spatial domain, the optimal distribution of material and its effective properties using the objective of minimum material resource or minimum compliance.

The most specific aspect of this structural optimization methodology is that the minimum of the objective function is sought by assuming a free parametrization of the material elastic tensor. Hence, it is sometime called Design by Free Parametrization of Material. Such as mentioned in the Section 3.4 of the book [5], the so-formulated optimization problem is general enough and “...encompasses the design of structural materials in a broad sense, predicting optimal structural topologies and shapes associated with the optimum distribution of the optimized material”.

In the following years, the mathematical basis and new numerical algorithms for the FMO technique have been developed. In fact, some formulations of FMO can be written as convex optimization problems which satisfy the criterion for guaranteeing uniqueness of the solution, as shown by Zowe et al. [6] and Kočvara et al. [7]. Additionally, Kočvara and coauthors have developed optimized algorithms mainly based on non-linear semi-definite programming procedures for solving very large

FMO problems, see Kočvara et al. [7] and Stingl et al. [8]. Furthermore, efficient primal-dual interior point methods for large-scale problems have been proposed and studied more recently by Weldeyesus and Stolpe [9].

Intrinsically associated with the FMO methodology is the inverse problem of the material micro-architecture design. In this case, the goal is to find a heterogeneous composite whose effective properties are similar to those required by the FMO solution. Important contributions to reach this objective have also been proposed in the 1990's, particularly in the papers of Sigmund ([10] and [11]), who has solved the inverse material design problem using a topology optimization procedure. In this sense, the density-based SIMP (Solid Isotropic Material with Penalization) method has proved to be a very effective tool for solving this kind of inverse homogenization problem.

A FMO technique jointly with inverse material design, as a global two-scale material design methodology, can be utilized as a weakly coupled procedure between the involved scales. First, a FMO technique is employed to compute the effective material properties at the large scale, i.e. at the structure length scale identified as the macro-scale, followed by a technique for designing the micro-structure of the heterogeneous composite. Such two-scale technique and variants were worked out by several authors and particularly utilized by Schury et al. [12]. Interestingly, this type of two-scale technique does not only provide an optimal material distribution at the macro-scale, but also the requested computational cost is accessible even for attacking 3D problems.

There is, however, an inherent difficulty associated with this two-scale methodology which is caused by the one-way coupling between scales. In fact, it is not possible to add well-founded mathematical constraints to the FMO formulation in order to guarantee the micro-structure attainability. Such as mentioned by Allaire in his book, [13], from the mechanical point of view, this issue is similar to answer the question on how to characterize the range of the effective properties obtained from a two-phase composite by varying its micro-structure. In this context, the micro-structure variation is understood as changing either the void fractions, the distributions of the constituent phases or their elastic properties. From the mathematical point of view, this issue corresponds to finding the G-closure of the set of effective elastic properties obtained from composites with all possible micro-structures, see also Cherkaev [14]. Milton and Cherkaev [15] have studied this problem and have determined that any positive definite tensor may be attained using sequential laminates under the condition that a stiff enough material exists. However, positive definite tensor bounds guaranteeing this property with less stringent conditions to that required by the Cherkaev and Milton analysis do not exist; for example when the stiffness of the composite phases have an upper finite limit. Therefore, this problem is an open issue at the present time.

More recently, there have been intents of including additional manufacture con-

straints to the FMO problem, such as described in Schury [16]. These constraints not only force a gradual spatial change of the effective material properties, but also they restrict the set of FMO solutions by avoiding the use of extreme materials at the cost of obtaining suboptimal solutions.

From this perspective, additional contributions could be expected by developing new procedures that help designing micro-architectures with a wide spectrum of attainable effective elasticity tensors. In this paper we emphasize this specific issue of the problem.

On the one hand, we adopt a FMO technique at the macro-scale to determine the material distribution and its effective elastic properties. On the other hand, we employ a topology optimization technique to solve the inverse micro-structure design problem. The technique adopted at the micro-scale is similar to the procedure explained in the Amstutz's works and uses the concepts of topological derivative and level-set function, see [17] and [18]. These two techniques are now well-established in the literature, and therefore, no new contributions on these procedures are revealed in this paper.

Instead, the essential contribution here aims to describe two new tools that aid to explore and design a range of periodic material micro-architectures. The principal ideas supporting these contributions are summarized as follows:

- i)* The first tool is addressed to define the shape of the unit-cell domain where the micro-structure material inverse homogenization problem is posed. Our numerical experience shows that adequate cell shapes increase the range of elasticity tensors that can be attained through simple micro-architecture topologies. In this sense, it should be noted that certain topologies may be hidden when only conventional square or rectangular cells subjected to periodic boundary conditions are taken.

The objective that we pursue here is to use a cell shape matching a unit-cell shape of the designed periodic material. So, by using the symmetry of the effective material properties, we conjecture that the stiff material of the composite is periodically distributed by following a pattern which can be assimilated to a Bravais lattice having the same class of symmetry as that of the target elasticity tensor. Then, the adopted cell for the topological design problem is a Voronoi cell of this Bravais lattice.

Although the use of polygonal cells for the material inverse design was analyzed in the past by Diaz and Benard [19], to the best of our knowledge, the use of Voronoi cells applied to topological design has not been previously considered in the literature.

- ii)* The second of these tools provides a procedure to choose an adequate stiff phase distribution within the Voronoi-cell. This configuration is then utilized

as the starting point for the topology optimization algorithm determining the final cell configuration.

A brief description of this paper is the following: the two-scale approach for the material micro-architecture design is briefly revisited in Section 2. Then, the taxonomy of the elastic materials obtained with the structural optimization technique is explored. This classification is utilized for the posterior development of the relevant topics in this paper.

Section 3 gives an overview of two FMO problems that are sequentially solved. Results in terms of extreme materials are analyzed in the same Section.

In Section 4, the adopted methodology for the micro-structure design is first presented. Then, Section 5 describes the new tools above mentioned.

In the last Section of the paper, we expose the conclusions. Two Appendices are finally added. The first Appendix describes the FMO discrete formulation and the algorithm to solve this problem. The second Appendix deals with issues related to symmetry properties of elastic materials. Also, the algorithm to compute the symmetry class and the normal form of an arbitrary elasticity tensor is there briefly exposed.

2 Overview of the two-scale based approach

In this work, the approach taken for the optimal material design of a plane elastic structure involves two length scales. The macro-scale length ℓ is of the same order of magnitude as that of the structure size, as shown in Figure 1. The micro-scale length ℓ_μ is of the same order of magnitude as that of the material micro-architecture characteristic length. We assume that $\ell_\mu \ll \ell$.

The macro-scale spatial domain is denoted Ω . It identifies the region where the structure is analyzed and where the optimal distribution of the graduated homogenized material is sought. The material at this scale is characterized by its effective properties, and its optimal distribution is sought by means of a FMO technique.

The material micro-architecture design is defined as an inverse homogenization problem after the optimal elastic effective properties at the macro-scale point are known. This inverse problem is solved with a topology optimization technique. The domain Ω_μ denotes the cell where the material is designed. The goal is to find the material distribution within this cell such that the homogenized elasticity tensor, \mathbf{C}^h , matches a target effective elasticity tensor provided by the FMO technique.

The vector \mathbf{x} , as shown in Figure 1, denotes the spatial position of a point at the macro-scale. Also, the vector \mathbf{y} identifies the spatial position of a point at the micro-scale.

Macro-stress and macro-strains are denoted $\boldsymbol{\sigma}$ and $\boldsymbol{\varepsilon}$, respectively. The same entities at the micro-scale are denoted $\boldsymbol{\sigma}_\mu$ and $\boldsymbol{\varepsilon}_\mu$. The key material property in this

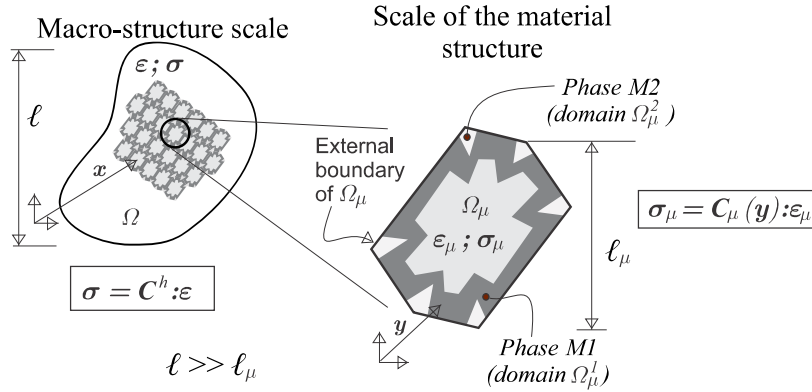


Figure 1: Two-scale material design. Notation and entities involved in the analysis. Macro-scale domain Ω and micro-cell Ω_μ .

work is the homogenized elasticity tensor \mathbf{C}^h at every point \mathbf{x} in Ω . This tensor is computed through a conventional homogenization technique. The elasticity tensors of the component phases at the micro-scale are identified with the symbol \mathbf{C}_μ .

It is convenient to remind the standard concepts of unit-cell and Representative Volume Element (RVE) utilized for computing effective elastic properties of periodic materials. A unit-cell in 2-D problems is the smallest area representing the overall behavior of the heterogeneous material, which, with all possible translation along the primitive vectors, fills the full plane without overlapping. Unit-cells have not arbitrary shapes, but they should be adapted in accordance with the periodic material micro-structure. Then, conventional periodic boundary conditions are a good choice for computing the homogenized properties utilizing these cells.

Arbitrary cell shapes, not matching unit-cell shapes, only represent the overall behavior of the material if they satisfy the condition of being RVEs. This situation occurs even forcing periodic boundary conditions. In this sense, for a given micro-structure, the RVE size should be much larger than the unit-cell size; its domain should comprise several unit-cells.

An additional important point to be also reminded here refers to Voronoi-cells. Periodically structured materials, such as crystals with their atomic arrangement represented through Bravais lattices, have one particular unit-cell whose geometry preserves the symmetry of the underlying lattice. This unit-cell is identified as the Voronoi-cell of the Bravais lattice.

2.1 Sequence of optimization problems

The two-scale material design procedure is performed in three successive stages.

- i) Initially, the FMO problem discussed in Section 3 is solved in the spatial region

Ω . This domain is chosen with a predefined geometry. The problem solution provides a graded distribution of effective properties given by the effective elasticity tensor $\hat{\mathbf{C}} \in \mathbb{S}^+$ in Ω , where \mathbb{S}^+ is the symmetric positive definite fourth order tensor set. Then, considering that $\text{tr}(\hat{\mathbf{C}})$ in the FMO formulation represents the pointwise material resource, the sub-domains of Ω satisfying the condition

$$\text{tr}(\hat{\mathbf{C}}) < \epsilon E_0 \quad (1)$$

are removed, and the original domain results in a smaller domain Ω^{red} . The parameter ϵ is a small value ($\epsilon \ll 1$), empirically adopted. The parameter E_0 is a reference Young's modulus, typically the modulus of the stiff phase of the designed composite.

Therefore, after the graded material has been defined in the complete domain through the FMO methodology, the heuristic condition (1) removes the sub-domains where the demanded material resource is low. A similar result can also be obtained using a more formal mathematical technique, for example, the one based on the topology optimization algorithm described in Giusti et al. [20]. Note that the topologies of Ω^{red} and Ω may be different.

- ii)* A second FMO problem is solved in the domain Ω^{red} by imposing the additional constraint,

$$(\hat{\mathbf{C}} - \delta \mathbf{1}) \in \mathbb{S}^+. \quad (2)$$

The scalar $\delta > 0$ is a small parameter ensuring that all the elasticity tensor eigenvalues are non-null. This constraint has been proposed by Schury [16] as a manufacture restriction.

Even when constraint (2) generates sub-optimal solutions, it facilitates the micro-structure design because it fixes lower bounds to the material properties. The effects of this constraint on the material design process are additionally discussed in sub-Section 3.2.

The solution of the second FMO problem provides the graded distribution of elasticity tensors, $\hat{\mathbf{C}}$, in Ω^{red} . Then, a target elasticity tensor, \mathbf{C}^* , representative of $\hat{\mathbf{C}}$ in a given sector of Ω^{red} is defined. The tensor \mathbf{C}^* is utilized to design the material micro-structure in that sector. Sub-Section 3.3 describes the criteria defining these sectors and how \mathbf{C}^* is computed.

- iii)* Finally, in a third stage, the micro-structure is designed using a topology optimization technique explained in Section 4. The design of the micro-structure is performed with \mathbf{C}^* as the target tensor.

The new tools for material design proposed in this paper are utilized in the third stage.

2.2 Characterization of linear elastic materials for optimal structures

Two remarkable features of linear elastic materials arising as the FMO problem solution are their symmetry and stability properties. In this sub-Section, we revisit both concepts because they are utilized to predict the shape and orientation of the cell Ω_μ .

2.2.1 Bi-mode and uni-mode unstable materials

Bi and uni-mode materials are special sub-classes of materials which frequently appear as solutions of optimal structural problems with design criterion related to minimal compliance or minimal material volume. In particular, bi-mode materials always arise as the optimal FMO solutions of structures subjected to a unique load system, see Bendsøe et al. [1]. But, even considering problems with multiple independent load systems ([2]), it is possible that optimal solutions would require bi or uni-mode materials in restricted regions of the structure. Both kinds of materials are particularly relevant in this work and analyzed in this Section.

Bi-mode materials are unstable materials having two easy (compliant) modes of deformation in a two-dimensional space and only one non-easy (hard) mode of deformation. Alternatively, uni-mode materials have one easy (compliant) mode of deformation and two non-easy (hard) modes of deformation. The elasticity tensors of bi and uni-mode materials have two and one null-eigenvalues, respectively. Hence, the names bi or uni-mode are given to these classes of materials.

Milton and Cherkaev [15] have coined these names in the context of linear elasticity, see also [21] where additional properties of these materials are analyzed.

Bi and uni-mode materials are special classes of linear anisotropic elastic solids. They are characterized by elasticity tensors ¹

$$\mathbf{C} = \sum_{i=1}^{n_m} \mathbf{S}_i \otimes \mathbf{S}_i \quad , \quad (3)$$

where \mathbf{S}_i are symmetric second order tensors, $n_m = 1$ for bi-mode and $n_m = 2$ for uni-mode materials, respectively. For uni-mode materials, \mathbf{S}_1 and \mathbf{S}_2 are orthogonal tensors. As usual, the symbol \otimes denotes the tensorial product. In the plane (x_1, x_2) , the eigenvector associated with the non-null eigenvalue in bi-mode materials is $\mathbf{S}_1/\|\mathbf{S}_1\|$.

¹Fourth order tensors are represented by matrices $\mathbf{R}^{3 \times 3}$ using the conventional Kelvin's notation. Consistent with this notation, symmetric second order tensors are represented by $\boldsymbol{\varepsilon} = [\varepsilon_{11}, \varepsilon_{22}, \sqrt{2}\varepsilon_{12}]^T$ for strains and $\boldsymbol{\sigma} = [\sigma_{11}, \sigma_{22}, \sqrt{2}\sigma_{12}]^T$ for stresses. From now on, we will indistinctly identify a fourth order tensor by its matrix representation.

Considering (3), for any strain $\boldsymbol{\varepsilon}$, the stresses $\boldsymbol{\sigma}$ result

$$\boldsymbol{\sigma} = \mathbf{C} : \boldsymbol{\varepsilon} = (\mathbf{S}_1 : \boldsymbol{\varepsilon}) \mathbf{S}_1 = -p \mathbf{S}_1, \quad (4)$$

where

$$p = -(\mathbf{S}_1 : \boldsymbol{\varepsilon}) \quad (5)$$

is a pseudo-pressure scalar term. In (4), the trace of the tensorial product is denoted by the symbol $(:)$.

In accordance with (4), bi-mode materials can only support stresses proportional to \mathbf{S}_1 , with the proportionality factor given by pseudo-pressures. Therefore, this material collapses when subjected to a different stress state.

2.2.2 Material symmetry

Symmetry classes of elastic materials are well established in the literature, see for example Ting [22]. In Appendix B we define the four symmetry classes for plane elasticity tensors and summarize the algorithm to compute them. The same algorithm also computes the rotation angle transforming an arbitrary elasticity tensor \mathbf{C} , expressed in the Cartesian coordinate system, to its normal form \mathbf{C}_N ².

Figure 2 sketches the diagram of sets for the four symmetry classes. Elements of these sets are elasticity tensors. We denote $O(2)$ for isotropic, D_4 for tetragonal, D_2 for orthotropic and Z_2 for anisotropic symmetries, respectively. From higher to lower symmetry classes, they are: $O(2) \subset D_4 \subset D_2 \subset Z_2$. In the Figure, the number of coefficients characterizing a generic elasticity tensor of the corresponding symmetry class is depicted in parenthesis.

Bi and uni-mode material sets are also included in the diagram. It can be seen the relationship between the stability properties of these materials as well as the number of null eigenvalues and the symmetry class to which they could belong to. It is remarked that bi or uni-mode materials with isotropic symmetry, $O(2)$, and bi-mode materials with tetragonal symmetry, D_4 , have elasticity tensors \mathbf{C}_N being proportional to those displayed in the Figure 2. They are characterized by only one parameter C_0 . Optimal structure solutions demanding bi-mode materials have been reported by Bendsøe et al. [1], see also Pedersen [23].

Orthotropic bi-mode materials have elasticity tensors with the normal form also shown in Figure 2. They are characterized by only two parameters. It is important to remark that a bi-mode isotropic material has an in-plane Poisson ratio $\nu = (C_N)_{1122}/(C_N)_{1111} = 1$. On the other hand, a tetragonal bi-mode material has a ratio: $(C_N)_{1122}/(C_N)_{1111} = -1$.

Important additional observations about this topic are:

²Elasticity tensors in normal axis are denoted with subindex N . The directions of the normal axes for a generic elasticity tensor \mathbf{C} are computed with the algorithm of Auffray et al. described in Appendix B.

- i)* bi-mode materials cannot be fully anisotropic (Z_2),
- ii)* bi and uni-mode materials are characterized with fewer parameters than those required by generic tensors in the corresponding symmetry class.

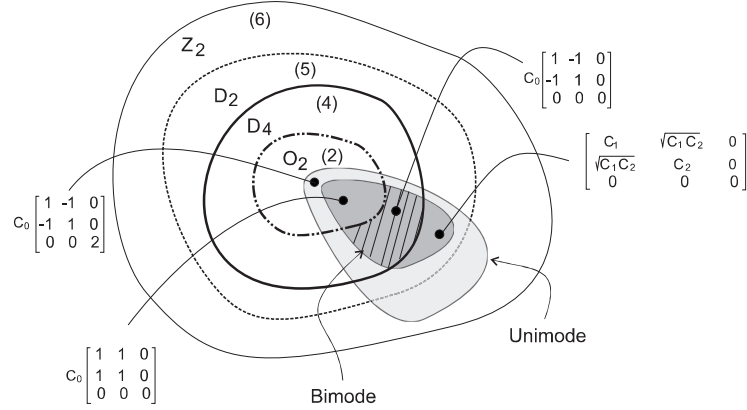


Figure 2: Diagram of symmetry class sets for plane elasticity tensors. Symmetry classes are denoted $O(2)$ for isotropic, D_4 for tetragonal, D_2 for orthotropic and Z_2 for fully anisotropic materials. The number of elastic coefficients defining the elasticity tensors in each class is shown in parenthesis. Bi and uni-mode material sets are also depicted. C_0 , C_1 and C_2 are material parameters.

3 Free Material Optimization at the macro-scale

Free Material Optimization (FMO) is a useful technique for obtaining the optimal distribution of material and effective elastic properties in a given spatial domain such that this material configuration satisfies a determined structural requirement. In the present context, the optimization criterion refers to minimum material resource and the structural requirement refers to the attainment of a limit compliance for a given external force.

3.1 Problem setting

Let us consider the equilibrium problem of an elastic body in Ω subjected to an external load \mathbf{f} . The space of displacement fields \mathbf{u} in equilibrium with the external forces, \mathcal{V}^{eq} , is:

$$\mathcal{V}^{eq} := \{ \mathbf{u} \mid \int_{\Omega} \nabla^s \mathbf{v} : \hat{\mathbf{C}} : \nabla^s \mathbf{u} dV - \langle \mathbf{f}, \mathbf{v} \rangle = 0 \quad \forall \mathbf{v} \in \mathcal{V} \}; \quad (6)$$

where the equilibrium condition is expressed through the conventional virtual work equation, with \mathcal{V} being the space of admissible virtual displacements and $\hat{\mathbf{C}}$ being the elasticity tensor.

In the present FMO formulation, the optimization problem consists of minimizing the structural material resource

$$\begin{aligned} & \min_{\hat{\mathbf{C}} \in \mathbb{S}^+, \mathbf{u} \in \mathcal{V}^{eq}} \int_{\Omega} \text{tr}(\hat{\mathbf{C}}) dV \\ \text{such that: } & \langle \mathbf{f}, \mathbf{u} \rangle \leq \bar{f}_u, \\ & \underline{\rho} \leq \text{tr}(\hat{\mathbf{C}}) \leq \bar{\rho}, \end{aligned} \quad (7)$$

where the term $\text{tr}(\hat{\mathbf{C}})$ represents the pointwise material resource and the design variables are the displacement field \mathbf{u} and the elasticity tensor $\hat{\mathbf{C}}$. Also, \mathbb{S}^+ is the space of symmetric positive semi-definite fourth order tensors, $\underline{\rho}$ and $\bar{\rho}$ are the lower and upper bounds imposed to the material resource, respectively. The lower bound $\underline{\rho}$ is a solvability condition imposed to avoid singularities in the structural equilibrium solution. Also, the upper bound $\bar{\rho}$ is a manufacturability condition that is chosen by considering the higher eigenvalue of the matrix representing the isotropic elasticity tensor of the stiff phase. This eigenvalue is proportional to the Young's modulus, E_0 , of the composite stiff phase. Then we take

$$\bar{\rho} = \beta E_0, \quad (8)$$

with $\beta < 3$ being an adimensional factor related to the volume fraction of the stiff phase. An empirical rule in material design indicates that the lower the parameter β , the easier is to find extreme materials with complex mechanism-like microstructures. In (7), the upper bound for the structural compliance, \bar{f}_u , is taken as the compliance computed with the structure constituted by a homogeneously distributed elastic material in Ω , with an elasticity tensor given by $(\beta/3)E_0\mathbf{1}$, where $\mathbf{1}$ is the identity fourth order tensor.

The optimal solution of problem (7) gives: *i*) the spatial distribution of $\hat{\mathbf{C}}$, *ii*) the symmetry class to which the material belongs to and *iii*) the magnitude of the elastic coefficients.

In structural optimization problems involving several independent load systems, the constraint (7)-b is replaced by

$$\sum_{k=1}^{n_{load}} w_k \langle \mathbf{f}_k, \mathbf{u}_k \rangle \leq \bar{f}_u; \quad (9)$$

where n_{load} is the number of load cases. The k -th load system is defined by the external force \mathbf{f}_k and \mathbf{u}_k is the associated displacement of the equilibrium solution,

w_k (with $w_k \geq 0$ and $\sum_{k=1}^{n_{load}} w_k = 1$) is a factor weighting each load system. and \bar{f}_u is an upper limit for the weighted average of the compliance.

In Appendix A, we summarize the discretization technique utilized to solve the present FMO formulation and give some details about the algorithm utilized to solve it.

3.2 Discussion of results obtained with the FMO technique

Discussions of the results obtained with the FMO technique are mainly addressed to analyze the stability, symmetry classes, and additional features of the optimal material properties. This analysis provides basic guidelines for taking adequate decisions in the posterior stage of micro-structure inverse design.

As an empirical rule in the present discussion, we keep in mind that materials demanding high effective shear stiffness jointly with effective in-plane Poisson ratio tending to -1 require the design of complex micro-structures.

3.2.1 First FMO problem

Four conventional structural optimization tests reported in the literature are presented. They are sketched in the first column of Figure 3 and are: *i*) L-shaped plate, *ii*) cantilever beam, *iii*) plate subjected to bending loads, all of them subjected to only one load system, f_1 . The test *iv*), is a plate subjected to three independent load systems, f_1 , f_2 and f_3 .

Second to fourth columns of Figure 3, as well as Figure 4, display the results of the four tests obtained with the FMO methodology and $\beta = 0.1$ in equation (8). These Figures show the color maps of the optimal distribution of the following fields:

- **Trace of the normalized elasticity tensors**, $\text{tr}(\hat{\mathbf{C}}/E_0)$, ranging from 0.1 to 6×10^{-5} . The material in regions with low values of this field can be removed.
- **Material symmetry classes**. In the tests subjected to only one load system (*i* to *iii*), the optimal materials determined with the FMO problem are bi-mode materials with symmetries D_4 or D_2 . In general, materials with isotropic symmetry $O(2)$ are not observed.

For the plate subjected to three independent load systems, the optimal solution gives materials with three non-null eigenvalues, compare Figure 3 and Figure 4. In this case, it is also interesting to observe large regions displaying uni-mode materials with full anisotropy (Z_2), as well as, extended regions with bi-mode materials.

- **Ratio** $(\hat{\mathbf{C}}_N)_{1122}/(\hat{\mathbf{C}}_N)_{1111}$. The material symmetry classes of optimum solutions computed in tests *i-iii*, display rather extended regions with tetrago-

nal (D_4) symmetry meaning that $(\hat{C}_N)_{1111} = (\hat{C}_N)_{2222}$. Therefore, in accordance with the comments remarked in sub-Section 2.2.2, the bi-mode materials in these regions should necessarily have an in-plane Poisson ratio of value $(\hat{C}_N)_{1122}/(\hat{C}_N)_{1111} = -1$.

A further analysis of the ratio $(\hat{C}_N)_{1122}/(\hat{C}_N)_{1111}$ in tests (*i* to *iii*) shows that the optimal solutions in large part of the structures demand auxetic materials. Roughly speaking, auxetic materials with ratios close to $(\hat{C}_N)_{1122}/(\hat{C}_N)_{1111} \approx -1$ requires the design of more complex micro-structures with mechanism-like topologies.

- **Smallest non-null eigenvalues of \hat{C}/E_0 .** Solutions corresponding to only one load system (tests *i* to *iii*) display two eigenvalues equal to zero in the complete structural domain indicating that a bimodal material is the optimal solution, such as reported by Bendsøe et al. [1]. Then, the map of the only one non-null eigenvalue is identical to the map of $\text{tr}(\hat{C}/E_0)$. We recall from equation (3) that bi-mode material properties have symmetry axes aligned with the principal stress and strain directions.

In Figure 4, we show the distribution of the three elasticity tensor eigenvalues obtained as result of the test *iv*. Zones with three non-null eigenvalues can be observed. However, there still exist regions with one and two close to zero eigenvalues.

3.2.2 Second FMO problem

Next, we analyze the results obtained with the second FMO problem with the addition of constraint (2) for the L-plate test. This problem is solved in the reduced domain Ω^{red} that results after adopting a tolerance $\epsilon = 0.015$ in expression (1). The so-reduced domain Ω^{red} is depicted in Figure 5-a.

We start the analysis by studying first the sensitivity of results respects to the parameters δ and β introduced in expressions (2) and (8), respectively. Let us consider the role played by parameter δ :

- On the one hand, δ is utilized to suppress solutions yielding extreme materials. This effect is notoriously shown in the FMO solutions for problems with only one load system. In these cases, we have already seen that the resulting elasticity tensors of the first FMO problem corresponds to bi-mode materials with symmetries D_2 and D_4 . Then, the addition of constraint (2) fixes a lower bound for the shear modulus, since $(\hat{C}_N)_{1212} \geq \delta/2$. Also, it fixes an upper bound for the ratio $\left|(\hat{C}_N)_{1122}/(\hat{C}_N)_{1111}\right|$. In fact, being $(\hat{C}_N)_{1111} \geq (\hat{C}_N)_{2222} \geq$

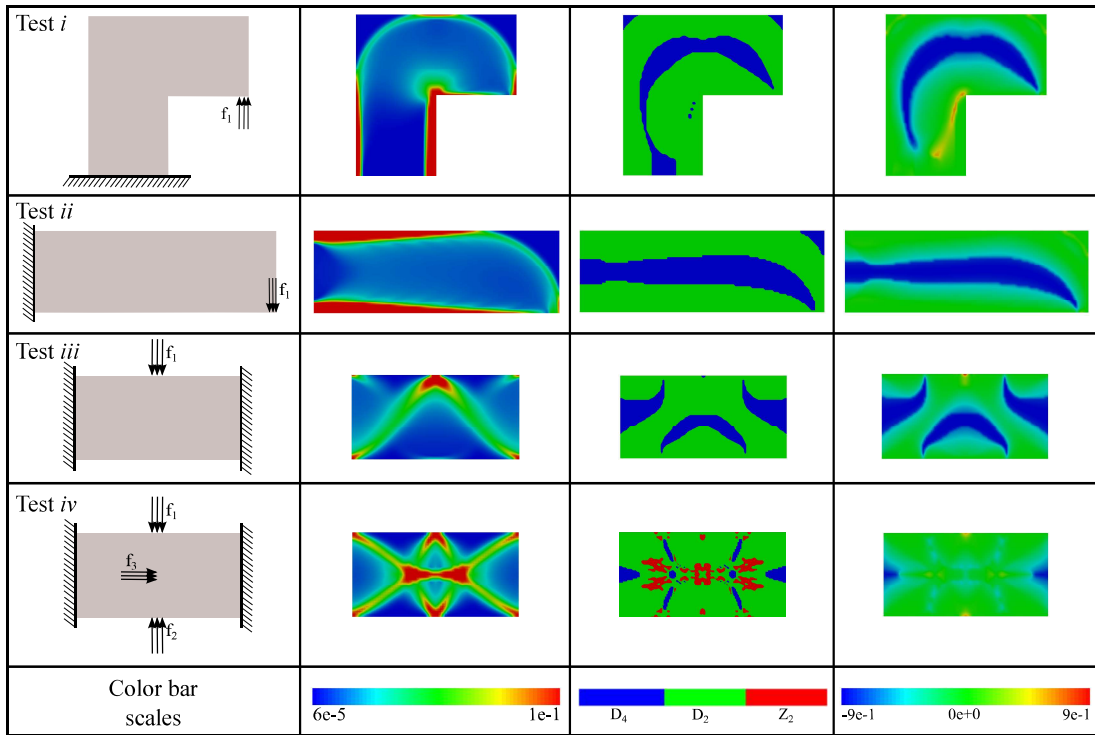


Figure 3: FMO results. *First column*: test description; *second column*: elastic tensor trace; *third column*: symmetry classes; *fourth column*: ratio $(\hat{C}_N)_{1122}/(\hat{C}_N)_{1111}$. The condition $(\hat{C}_N)_{1122}/(\hat{C}_N)_{1111} < 0$ defines the regions where the optimal solution requires auxetic materials (zones in blue).

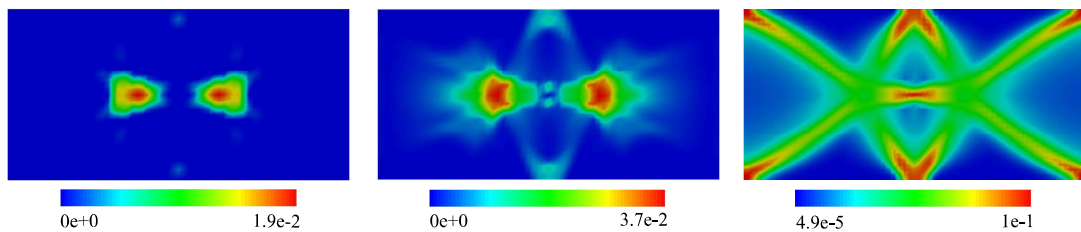


Figure 4: Eigenvalues of the elastic tensors for the plate with three load systems. Left to right: from smallest to largest eigenvalues.

Table 1: L-plate test solved with the second FMO problem, $\beta = 0.1$ and different values of parameters δ .

δ/E_0	$\min \int_{\Omega^{red}} \text{tr}(\hat{\mathbf{C}}/E_0)dV$	$\min \left(\frac{(\hat{C}_N)_{1122}}{(\hat{C}_N)_{1111}} \right)$	$\max \left(\frac{(\hat{C}_N)_{1122}}{(\hat{C}_N)_{1111}} \right)$
0.	1.89e2	-1.00	1.00
0.020	2.27e2	-0.76	0.95
0.025	2.37e2	-0.71	0.93
0.033	2.52e2	-0.64	0.92
0.040	2.62e2	-0.52	0.65

δ , it results

$$\left| \frac{(\hat{C}_N)_{1122}}{(\hat{C}_N)_{1111}} \right| \leq \sqrt{\left(\frac{(\hat{C}_N)_{2222}}{(\hat{C}_N)_{1111}} - \frac{\delta}{(\hat{C}_N)_{1111}} \right) \left(1 - \frac{\delta}{(\hat{C}_N)_{1111}} \right)} \leq 1. \quad (10)$$

- On the other hand, by comparing with the original FMO problem, the constraint (2) produces sub-optimal solutions. The larger the value δ the higher the optimal cost function value.

Both effects are confirmed by analyzing the results shown in Table 1. This Table displays the optimal cost functions obtained with different values of δ . In the same Table, we also show the corresponding lower and upper values of $(\hat{C}_N)_{1122}/(\hat{C}_N)_{1111}$ in Ω^{red} . We can see that, as δ gets larger, the optimal cost function increases and the extremal values of the field $|(\hat{C}_N)_{1122}/(\hat{C}_N)_{1111}|$ are closer to zero.

Also, in order to understand the connection between the parameters β and δ , it should be kept in mind that designing complex materials could be facilitated by taking smaller volume fractions of the stiff phase, or similarly, smaller values of β , see the discussion about this issue in Sigmund [24]. So, the parameters δ and β have to be adjusted after an adequate trade-off between optimality and manufacturability requirements.

Finally, the parameter ϵ , defining the size of the domain Ω^{red} , is related to δ , in the sense that it should be taken $\epsilon < \delta/E_0$. However, this parameter plays a less important role in the second FMO problem.

Result obtained with the second FMO problem

Figure 5-b displays the field $\text{tr}(\hat{\mathbf{C}}/E_0)$ on the domain Ω^{red} of the L-plate problem, only one load system, obtained with $\delta = E_0/25$ and $\beta = 0.1$.

Figure 5-c and d show the color maps of the optimum material symmetry classes and their ratio $(\hat{C}_N)_{1122}/(\hat{C}_N)_{1111}$. The distribution as well as the maximum and

minimum values are slightly different from those obtained with the original FMO problem on Ω depicted in Figure 3. Notably in this case, the range of values $(\hat{C}_N)_{1122}/(\hat{C}_N)_{1111}$ are limited to $-0.52 < (\hat{C}_N)_{1122}/(\hat{C}_N)_{1111} < 0.65$, which is a much narrower interval to that displayed by the original FMO solution ranging between $-1 \leq (\hat{C}_N)_{1122}/(\hat{C}_N)_{1111} \leq 1$, see Figure 3. Also, in accordance with the constraint (2), the smallest eigenvalue of the elasticity tensor is δ .

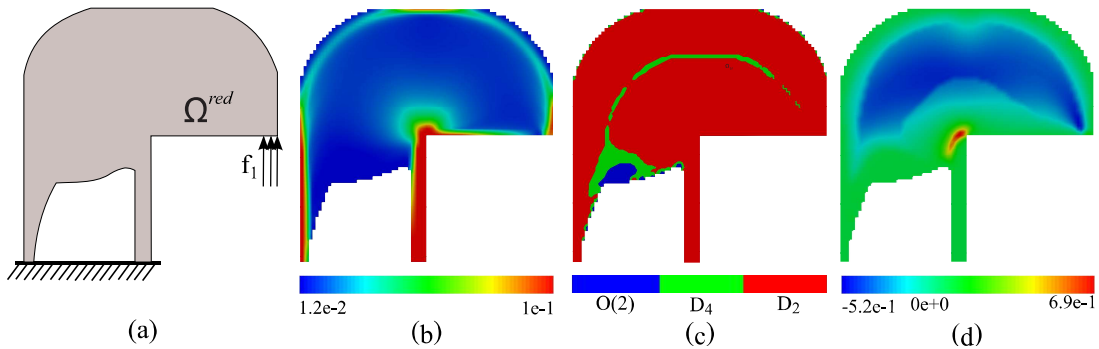


Figure 5: L-plate test solved with the second FMO problem. a) Reduced domain Ω^{red} after adopting $\delta = E_0/25$. b) Trace of the elasticity tensor ($\text{tr}(\hat{C}/E_0)$); c) material symmetry classes; d) ratio $(\hat{C}_N)_{1122}/(\hat{C}_N)_{1111}$

3.3 Domain partition criterion for material design

Once solved the second FMO problem, the structure domain Ω^{red} is partitioned into disjoint sectors with similar effective material properties. The criterion to define this partition is next discussed.

Given the fields: $\text{tr}(\hat{C}/E_0)$ and $(\hat{C}_N)_{1122}/(\hat{C}_N)_{1111}$, we take the intervals defined by their extreme values:

- a) $\mathcal{I}_{tr} := [\min(\text{tr}(\hat{C}/E_0)); \max(\text{tr}(\hat{C}/E_0))]$,
- b) $\mathcal{I}_{Poi} := [\min\left(\frac{(\hat{C}_N)_{1122}}{(\hat{C}_N)_{1111}}\right); \max\left(\frac{(\hat{C}_N)_{1122}}{(\hat{C}_N)_{1111}}\right)]$.

and divide them in N_{tr} and N_{Poi} proportional sub-intervals, respectively. Also, we take the N_{sym} different symmetry classes of the elasticity tensors found in the FMO solution. With these sub-intervals and classes of symmetries, we can define $N_{tr} \times N_{poi} \times N_{sym}$ sets of elastic properties sharing similar values. Then, it can be defined a natural map relating the $N_{tr} \times N_{poi} \times N_{sym}$ sets of elastic properties to sectors in Ω^{red} whose points have effective elastic properties lying within the range of the associated sets, with similar elastic properties: $\text{tr}(\hat{C}/E_0)$, $(\hat{C}_N)_{1122}/(\hat{C}_N)_{1111}$ and symmetry class. Then, these sectors are denoted Ω_i^{red} with $i = 1, \dots, n_s$ and n_s is the number of sectors satisfying $n_s \leq N_{tr} \times N_{poi} \times N_{sym}$.

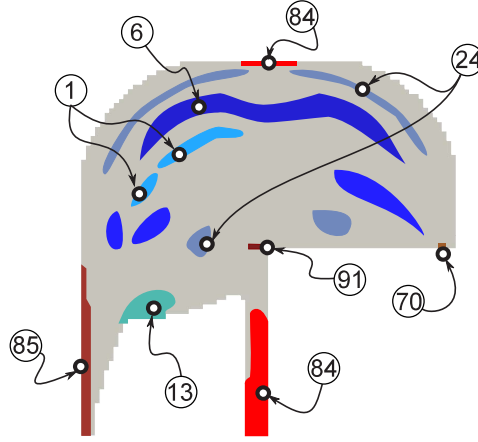


Figure 6: Domain partition criterion for the material micro-structure design, $N_{tr} = N_{Poi} = 13$, $N_{sym} = 3$, and $n_s = 91$. Only a small number of sectors Ω_i^{red} (with $i = 1, 6, 13, 24, 70, 84, 85, 91$), defined by similar effective elastic properties are identified in colors.

For the L-plate test and taking $N_{tr} = N_{poi} = 13$ and $N_{sym} = 3$, it results $n_s = 91$. Some of these sectors are identified in Figure 6.

Finally, for every sector, a representative elasticity tensors \mathbf{C}_i^* can be computed as the average

$$\mathbf{C}_i^* = \frac{1}{|\Omega_i^{red}|} \int_{\Omega_i^{red}} \hat{\mathbf{C}}_N dV ; \quad \forall i = 1, \dots, n_s \quad . \quad (11)$$

where $|\Omega_i^{red}|$ is the area of the corresponding i -th sector.

The tensor³ \mathbf{C}^* is taken as the target tensor to design the micro-structure using the algorithm described in the following Section.

4 Micro-architecture design

Let us consider a two-phase composite constituted by a periodic distribution of a stiff phase M1 and a soft phase M2. Figure 7 represents the micro-cell of the periodic composite. We seek the distribution of phases M1 and M2 within the micro-cell such that the homogenized elasticity tensor $\mathbf{C}_N^{h,4}$, of this composite material, is identical to the target elasticity tensor \mathbf{C}^* derived from the treatment given to the FMO problem solution in the previous Section.

³In the following development, sub-index i identifying the sector of Ω_i^{red} is dropped out of the notation.

⁴The micro-structure design is performed in the normal basis.

This goal is reached by using an inverse homogenization approach that is formulated as a Topology Optimization Problem (TOP). The TOP is solved in a pre-defined micro-domain Ω_μ with the algorithm proposed by Amstutz and Andr a [17] and Amstutz et al. [18], see also Lopes et al. [25] and M endez et al. [26].

The TOP uses a computational technique for evaluating the homogenized elasticity tensor \mathbf{C}_N^h , the topological derivative concept of the homogenized elasticity tensor and a function describing the distribution of phases in the micro-cell. The zero-level set of this function represents the interfaces within the cell.

In this work, we only remark some aspects of the TOP which have been particularly adapted for solving the present inverse homogenization problem. They are: the TOP cost function, the imposed constraints and the augmented Lagrangian technique to solve it. Other more conventional aspects of the topology optimization algorithm, such as the topological derivative expression, are not addressed here because they have been extensively treated in the above-referenced literature.

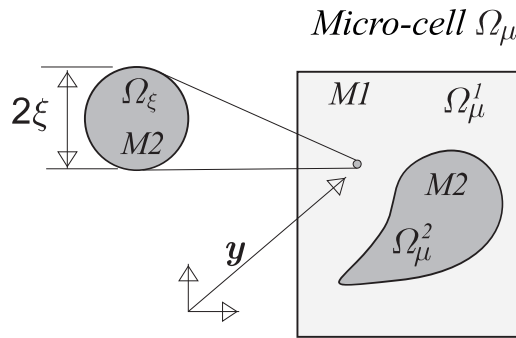


Figure 7: Original micro-cell problem with a material distribution perturbation consisting of introducing a ball Ω_ξ of soft phase within the stiff phase. The radius of the infinitesimal ball is ξ .

4.1 Inverse material design as a TOP

Let us consider a micro-cell, Ω_μ , of the periodic composite constituted by isotropic elastic phases M1 and M2 occupying the domains Ω_μ^1 and Ω_μ^2 , respectively. See Figure 7. The corresponding elastic tensors of both phases are $\mathbf{C}_\mu^2 = \gamma \mathbf{C}_\mu^1$ with γ being a contrast factor. The characteristic and contrast functions in Ω_μ are defined by

$$\chi(\mathbf{y}) = \begin{cases} 0 & \forall \mathbf{y} \in \Omega_\mu^2 \\ 1 & \forall \mathbf{y} \in \Omega_\mu^1 \end{cases} \quad ; \quad \rho(\mathbf{y}) = \begin{cases} \gamma & \text{if } \chi = 0 \\ 1 & \text{if } \chi = 1 \end{cases} \quad , \quad (12)$$

respectively. Evidently, the homogenized elasticity tensor \mathbf{C}^h of the composite depends on the way in which phases M1 and M2 are distributed in Ω_μ . This dependence is made explicit by introducing the notation $\mathbf{C}^h(\chi)$.

Next, we redefine the micro-architecture inverse design problem as a topology optimization problem expressed as follows: given the target effective elasticity tensor \mathbf{C}^* , find the characteristic function χ satisfying

$$\begin{aligned} \min_{\chi} \int_{\Omega_{\mu}} \chi \, d\Omega \\ \text{such that: } \|\mathbf{C}_N^h(\chi) - \mathbf{C}^*\| = 0. \end{aligned} \quad (13)$$

The cost function represents the stiff phase volume fraction. In particular, considering that the soft phase is void, the problem (13) identifies a minimum weight problem.

4.2 Algorithm for solving the TOP

The TOP (13) can be solved by introducing a level set-function $\psi \in C^0(\Omega_{\mu})$ defined by

$$\psi(\mathbf{y}) = \begin{cases} < 0 & \forall \mathbf{y} \in \Omega_{\mu}^2 \\ > 0 & \forall \mathbf{y} \in \Omega_{\mu}^1 \\ 0 & \text{in the interfaces} \end{cases}, \quad (14)$$

and utilizing an augmented Lagrangian technique. In this case, the problem is rewritten as follows

$$\max_{\lambda} \min_{\psi} \mathcal{T}(\psi, \lambda), \quad (15)$$

with:

$$\mathcal{T}(\psi, \lambda) = \int_{\Omega_{\mu}} \chi(\psi) \, d\Omega + \lambda(\|\mathbf{C}_N^h(\psi) - \mathbf{C}^*\|) + \frac{\alpha}{2}(\|\mathbf{C}_N^h(\psi) - \mathbf{C}^*\|)^2 \quad (16)$$

where λ is the the constraint Lagrange multiplier and α is the penalty parameter.

The algorithm for solving the problem (15) utilizes two nested loops. In an internal loop, the objective function \mathcal{T} is minimized by holding fixed λ and α . This loop, with index denoted k , consists of a level-set function-based iteration. While, an external loop, with index denoted l , modifies iteratively λ .

The minimum of \mathcal{T} in the internal loop is searched with a descent direction algorithm. For problem (15), the topological derivative is given by

$$D_{\psi} \mathcal{T}(\psi, \lambda) = 1 - \left((\lambda - \alpha \|\mathbf{C}_N^h - \mathbf{C}^*\|) \frac{(\mathbf{C}_N^h - \mathbf{C}^*) : D_{\psi} \mathbf{C}^h}{\|\mathbf{C}_N^h - \mathbf{C}^*\|} \right) \quad (17)$$

where $D_{\psi} \mathbf{C}^h$ is the topological derivative of the homogenized elasticity tensor, see [18] for an additional description of this term. Then, we define the function :

$$g(\mathbf{y}) = \begin{cases} -(D_{\psi} \mathcal{T}) & \text{if } : \psi < 0 \\ +(D_{\psi} \mathcal{T}) & \text{if } : \psi > 0 \end{cases}, \quad (18)$$

The updating formula for ψ , at the $(k + 1)$ -th internal loop, is defined by

$$\psi^{k+1} = \psi^k + \tau g, \quad (19)$$

with the scaling factor τ being determined by means of a line search technique.

In the $(l + 1)$ -th external loop, the Lagrange multiplier λ is updated using the Uzawa algorithm

$$\lambda^{l+1} = \max(0, \lambda^l + \alpha \|\mathbf{C}_N^h - \mathbf{C}^*\|). \quad (20)$$

The penalty parameter α is held fixed during the full process.

A local optimality criterion of problem (15), see Amstutz [27], is given by the condition

$$D_\psi \mathcal{T} > 0 \quad ; \quad \forall \mathbf{y} \in \Omega_\mu \quad (21)$$

which can be implemented by verifying the equality

$$\arccos \left[\frac{\int_{\Omega_\mu} g \psi \, dV}{\|g\|_{L^2} \|\psi\|_{L^2}} \right] = 0. \quad (22)$$

5 Methodology for searching the optimal micro-structure

Leaving aside the issue related to existence of solutions⁵, finding one solution of problem (15) may be difficult, especially when extreme materials are designed. The search of a solution with the algorithm described in sub-Section 4.2 is facilitated by following two procedures that are summarized in sub-Section 5.1 and 5.2.

5.1 Selection of the micro-cell shape Ω_μ

The shape of the domain Ω_μ is an implicit variable utilized in the inverse homogenization problem (13) that should be defined in advance. Considering that problem (13) searches for an optimal periodic micro-structure, this variable plays a major role to find an adequate material micro-architecture adjusting the target elasticity.

A good decision is to choose Ω_μ coinciding with the shape of a micro-structure unit-cell. However, in view that the periodic micro-structure is unknown at the moment of solving the inverse homogenization problem, we conjecture that the periodic micro-cell Ω_μ coincides with the shape of the Voronoi Cell of a Bravais lattice related to a crystal which elasticity tensor has the same symmetry as that displayed by the target tensor \mathbf{C}^* .

⁵As previously mentioned, this issue can be mitigated through the handling of the parameter δ in equation (2).

In Figure 8, we show the only five different Bravais lattices in 2D and their associated symmetry classes. A Bravais lattice is fully described with the primitive vectors \mathbf{a}_1 and \mathbf{a}_2 . Therefore, Bravais lattices could be described with two parameters, the ratio $\omega = \|\mathbf{a}_2\|/\|\mathbf{a}_1\|$ and the angle $\varsigma = \arccos[(\mathbf{a}_2 \cdot \mathbf{a}_1)/(\|\mathbf{a}_2\|\|\mathbf{a}_1\|)]$. Additional information about this topic can be found in the book [28].

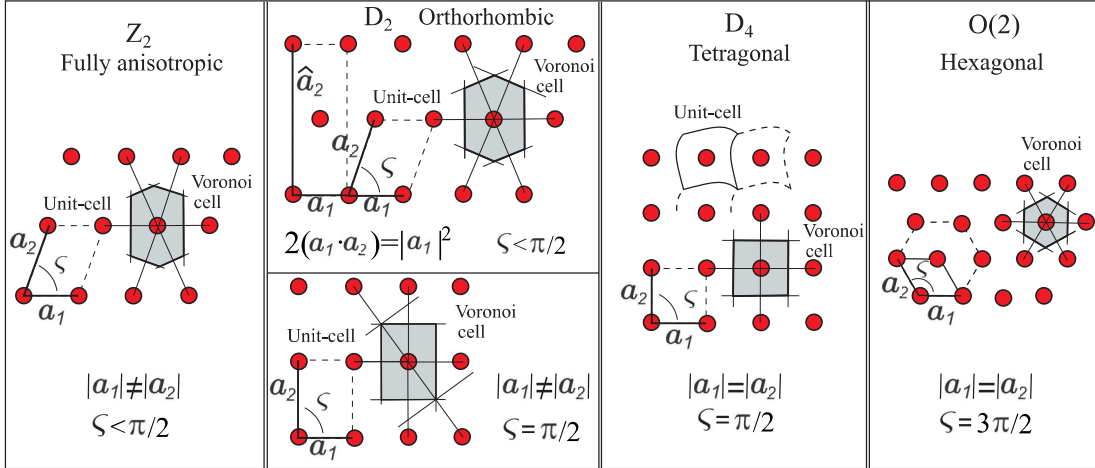


Figure 8: Bravais lattices and Voronoi cells (Wigner–Seitz cells) for the material symmetry classes in plane problems. There are only five Bravais lattices in two dimensions, see Kittel [29].

Also, in the same Figure, it can be observed that several unit-cells are associated with a given Bravais lattice, see for instance the unit-cells of the lattice with D_4 symmetry.

From all possible unit-cells, our interest lies in the Voronoi cells (Weigner-Seitz cells) also depicted in the Figure. Voronoi-cell shapes preserve the symmetry of the underlying lattice. Observing the lattice with D_4 symmetry, horizontal and vertical directions are axes of symmetry for the lattice, however, they are not symmetry axes for all the unit-cells. Instead, the Voronoi-cell is symmetric respect to both axes, as well as to rotations of $\pm 90.deg$.

What is more important for the topology optimization problem is that the symmetry class of the homogenized elasticity tensor can be guaranteed by distributing the material within a Voronoi-cell with certain spatial symmetry prescribed according to each type of lattice. So, following this criterion, we force the material distribution defined by the level-set function in the iterative algorithm of sub-Section 4.2 to satisfy the rotational or reflection symmetries displayed in Figure 9.

Figure 10-a displays the plane ω, ς in R^2 , where each pair ω, ς define a Bravais lattice. In gray, we show a bounded space of points with coordinates (ω, ς) defining the full set of all possible Bravais lattices. This reduced space is found by applying symmetry conditions to Bravais lattices. Notice, for example, that the lattice repre-

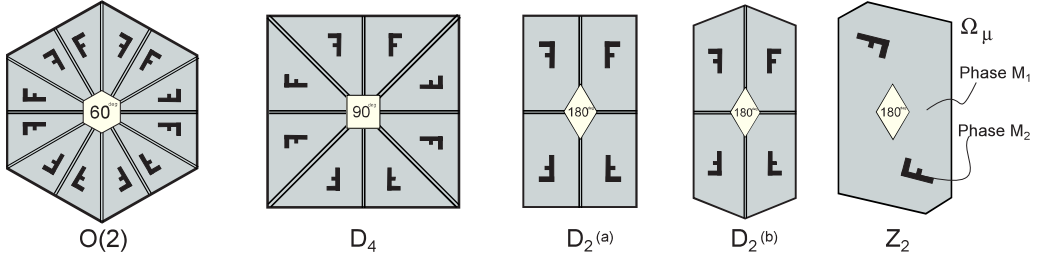


Figure 9: Voronoi-cell of a two-phase composite material. Planes and angles of symmetry utilized in the topology optimization algorithm for material distribution. The central symbol indicates the rotation angle preserving the symmetry. Reflection planes are symbolized with double segments.

sented in the Figure 10-b by the point denoted W' , with coordinates $(0.967, 75.deg)$, is the same lattice as that represented by the point denoted W with coordinates $(0.5, 30.deg)$.

Figure 10-c shows, in the same bounded space, the Voronoi cells associated with different points and the corresponding symmetry classes of these lattices. So, in the case that the target elasticity tensor \mathbf{C}^* has symmetry D_2 or D_4 , as it generally happens in FMO problem solutions with only one load system, it should be sufficient to restrict the search of the Ω_μ shape to some of the Voronoi-cells represented by the set of parameter ω, ς lying along the boundary of the gray region.

An additional criterion to determine which point (ω, ς) of this set is the most convenient one, is described in the following sub-Section.

5.2 Additional criteria to choose the micro-cell shape and the initial material configuration in Ω_μ

The criteria for choosing a particular Voronoi-cell of the space (ω, ς) , as well as an adequate distribution of material within this cell which can be taken as the initial configuration for the iterative algorithm solving the problem (13), are summarily explained here. A full description of this procedure is given in [30].

Initially, an off-line computation of several homogenized elasticity tensors is performed. These results are used to build a database of homogenized elastic tensors.

The homogenized elastic tensors stored in the data base are the results of several micro-cells with varying shapes and material configurations, such as described in the following items:

- Voronoi-cells with lattice parameters ω and ς sweeping the entire range of values depicted in gray in Figure 10-a;
- two material configurations denoted pattern A and B in Figure 10d-e. The material configuration of pattern A corresponds to equal thickness bars of solid

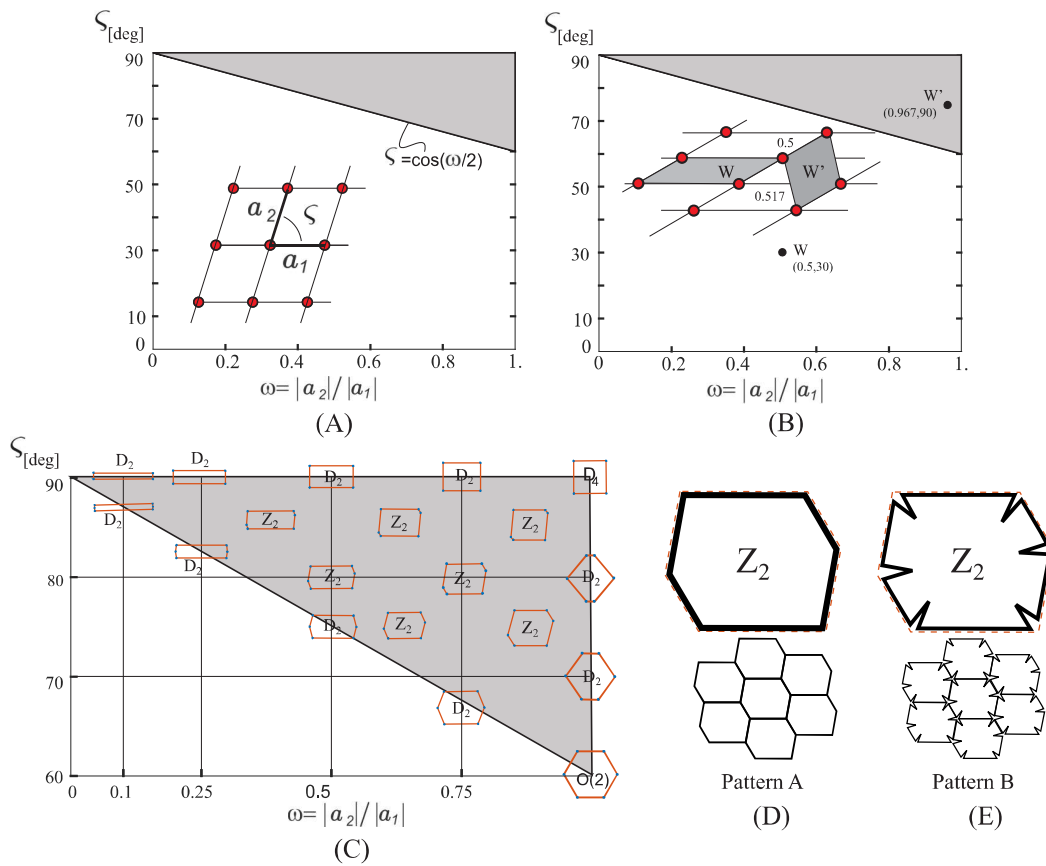


Figure 10: Space of parameters ω, ζ and micro-cell shapes. a) Bounded space of parameters ω, ζ identifying the complete set of Bravais lattices; b) a Bravais lattice can be represented by two different points, W' and W , in the space ω, ζ ; c) Voronoi cells and symmetry classes; d) and e) material distribution patterns A and B for determining the map $C_{db}^h(\omega, \zeta, f, P)$

material placed on the boundaries of the cells. The pattern B also corresponds to equal thickness bars placed on the boundaries of the cells but with a re-entrant configuration.

- several volume fractions f of solid material. This parameter f determines the bar thickness in each case.

Therefore, all computed homogenized elasticity tensors in the database can be characterized by four parameters: ω and ς , defining the Voronoi-cell shape, the solid volume fraction f and P defining the “Pattern” A or B. We identify each database entry with the notation $\mathbf{C}_{db}^h(\omega, \varsigma, f, P)$.

We recall that auxetic materials can be built with re-entrant configurations of bars, see Kolken and Zadpoor [31]. A profuse literature about honeycomb re-entrant auxetic materials exists, see for example Fu et al. [32] and references cited therein. The fact of capturing materials with negative ratios $(C_{db}^h)_{1122}/(C_{db}^h)_{1111}$ is the reason why we include pattern B in the database.

The database is built with a bar material having a normalized Young’s modulus⁶ $E = 1$. and Poisson ratio $\nu = 0.3$. Several values of f are used. We take approximately $6e3$ points to sweep the reduced domain in the plane (ω, ς) . Therefore, the database stores more than $1e5$ homogenized elasticity tensors.

Partial results of this database corresponding to the patterns A, B and $f = 0.05$ are depicted in Figure 11. These colored maps show in column: a) the maximum eigenvalue of the homogenized elasticity tensors, b) the ratios $(C_{db}^h)_{1122}/(C_{db}^h)_{1111}$ and c) the normalized shear stiffness $(C_{db}^h)_{1212}/(C_{db}^h)_{1111}$. As expected, the ratio $(C_{db}^h)_{1122}/(C_{db}^h)_{1111}$ of pattern B shows a large region of parameters ω, ς defining auxetic micro-architectures. The maximum eigenvalue gives an idea of the maximum stiffness displayed by the respective configuration. Also, note the connection between the ratio $(C_{db}^h)_{1122}/(C_{db}^h)_{1111}$ and the shear stiffness for different configurations.

With this database, the most adequate micro-cell shape and material distribution is adopted by using the criterion

$$\zeta = \arg \left\{ \min_{\mathbf{C}_{db}^h} \|\mathbf{C}_{db}^h(\zeta) - \mathbf{C}^*\| \right\}; \quad \text{where } \zeta := \{\omega, \varsigma, f, P\}, \quad (23)$$

which defines the instance of the database that is closer to the target elasticity tensor. The search of the minimum in (23) is restricted to the set of parameters (ω, ς) whose lattices have the same symmetry as \mathbf{C}^* .

⁶For all configurations displayed in this study, where the soft phase is void, the homogenized elasticity tensor is proportional to Young’s modulus of the stiff phase.

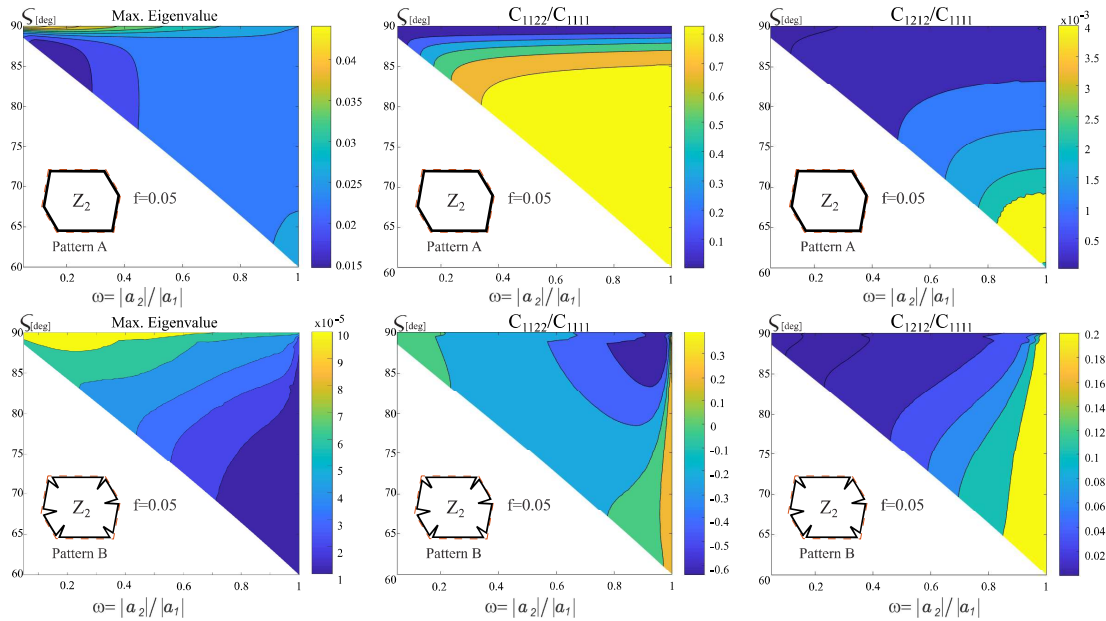


Figure 11: Maps of homogenized elastic properties of Voronoi cells parameterized with ω and ς , stiff material is distributed according to the patterns A and B and volume fraction of the stiff phase is $f = 0.05$.

5.3 Results

5.3.1 L-panel with one load system

Figure 12 shows the micro-structures computed with the explained design methodology. The results correspond to nine sectors of the L-panel denoted 1, 13, 24, 70, 72, 80, 84, 85 and 91, respectively. The unit-cells computed for these sectors are depicted such that the horizontal direction coincides with one of the homogenized tensor normal bases. In the same Figure, an assembly of several cells is also shown but rotated to the global Cartesian directions. The angle $-\theta$ transforms the normal basis direction to the global Cartesian one. Therefore, θ transforms $\hat{\mathbf{C}}$ into $\hat{\mathbf{C}}_N$, recalling that $\hat{\mathbf{C}}_N$ is used to compute equation (11). This angle θ is determined for every point of the L-panel.

Figure 13 compares the micro-cells gathered from the database and those obtained as solution of the TOP. The micro-cells depicted in the Figure correspond to the Sectors 1, 13, 24, 80 and 85. Micro-cells gathered from the database, using the procedure (23), are adopted as the initial configuration for the iterative topology optimization algorithm. Their homogenized elasticity tensor are denoted \mathbf{C}_{db}^h . Alternatively, the homogenized elasticity tensor computed with the micro-cells being the solution of the TOP are denoted \mathbf{C}_N^h .

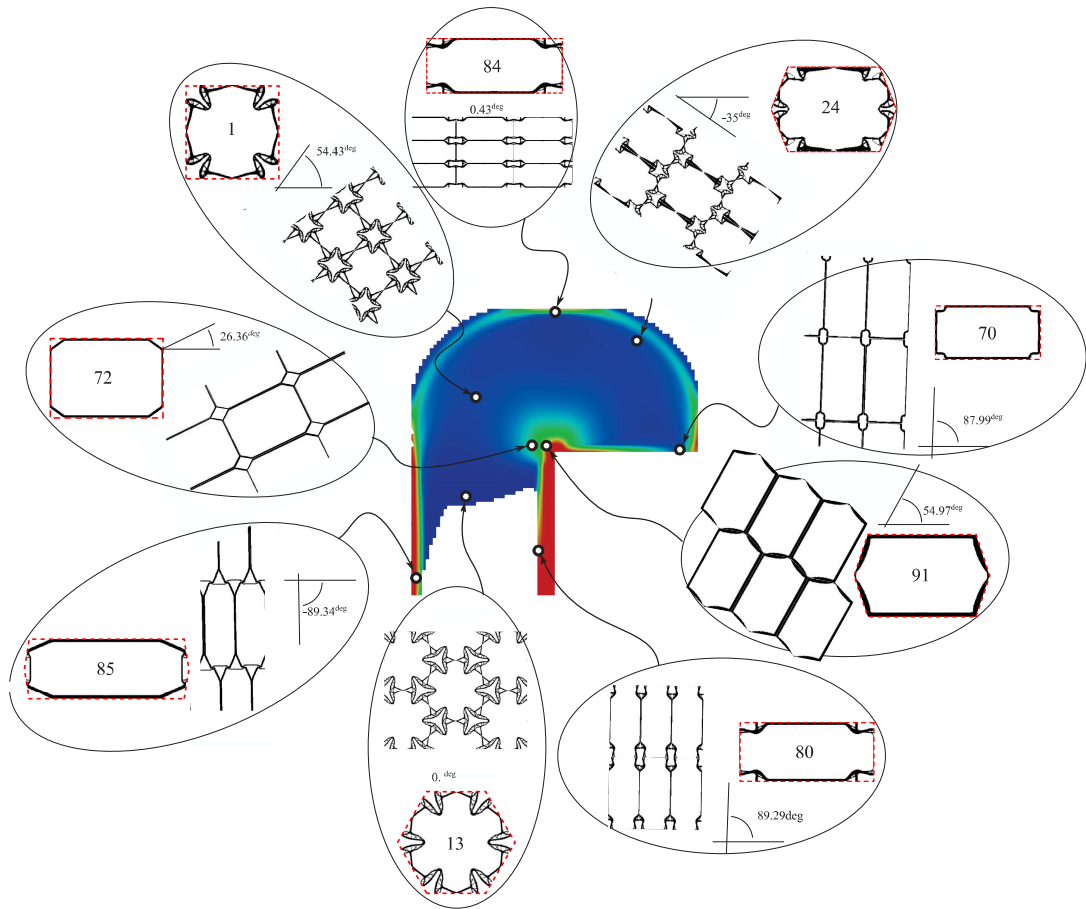


Figure 12: Computed micro-cells for several sectors of the L-panel test. The Cartesian basis of the micro-cells coincides with the normal basis. Assembled micro-cells are rotated to the physical directions in each sector.

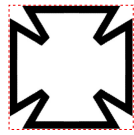
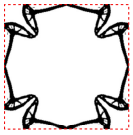
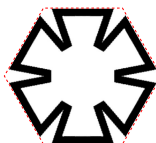
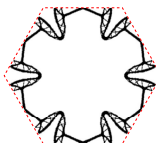
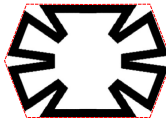
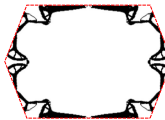




D_4	1		
$O(2)$	13		
D_2	24		
D_2	80		
D_2	85		

Figure 13: L-panel test, micro-structure design with the TOP. First column reveals the symmetry class of the target elastic tensor. Second column denotes the designed Sector. Third column depicts the micro-cells taken from the database as initial configurations for the topology optimization algorithm. Fourth column depicts the micro-cells obtained as solution of the topology optimization algorithm.

Note that the micro-architecture configurations remain rather simple and almost similar to the initial configurations gathered from the database. Also, observe that the micro-architectures in all sectors are honeycomb-like structures, but the cell shapes change notably in different sectors.

Even when a given sector of the L-panel has similar elastic properties, in accordance with the criterion adopted to define them, explained in the previous sub-Section, sectors have non-uniform distribution of the normal basis directions. Therefore, the designed representative micro-cell for one sector has to be rotated to the physical directions with the angle $-\theta$ at every point of the structure. We evidence this result in Figure 14. There, we depict the designed micro-structure for this sector in the physical directions for an identical sector which has been designed with a

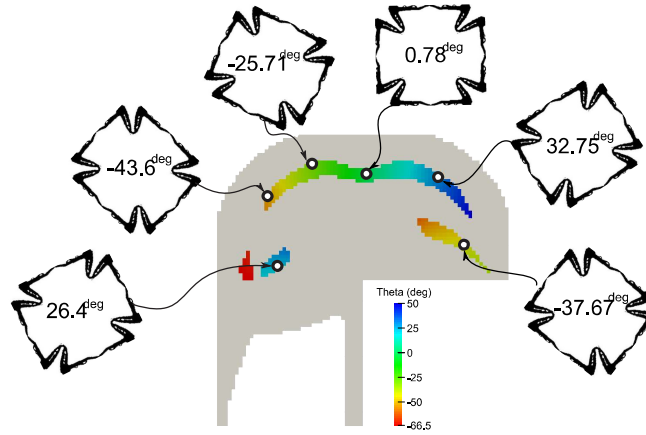


Figure 14: Resulting micro-structure of Sector 6 rotated to the physical directions. The rotation angle $-\theta$ is shown in accordance with the color scale.

unique micro-cell.

Table 2 displays the components of the target elasticity tensor \mathbf{C}^* , \mathbf{C}_{db}^h and \mathbf{C}_N^h in the mentioned sectors, respectively.

Note that, even when the initial configuration value \mathbf{C}_{db}^h is close to the target one, the optimization algorithm improves notably the results even without changing substantially the material distribution of the initial configuration. The last column in this Table identifies the volume fraction of the gathered and solved micro-cells.

Note also that from Figure 12 and Table 2, the Sector 13 requires a material with isotropic symmetry $O(2)$, as well as, an elasticity tensor with zero Poisson ratio and low stiffness. In this case, the re-entrant micro-structure designed with the present procedure facilitates the attainment of effective properties with almost zero Poisson ratio.

5.3.2 Plate subjected to three load systems

Figure 15 shows the micro-structures computed for two sectors of the plate subjected to three independent load systems.

The optimal structural result is taken from the first FMO problem solution, see Figure 3, test *iv*. In this case, material with symmetry Z_2 is found in the solution of the FMO problem even without including constraint (2). As the most challenging cases, we design the micro-structures of two points where the ratio $|C_{1112}^*/C_{1111}^*|$ is maximum. One case corresponds to a tensor with one null eigenvalue. The other case corresponds to a tensor with three non-null eigenvalues.

Figure 16 compares the micro-cells taken as initial configurations of the topology optimization algorithm with those obtained as solutions of the TOP. Sectors shown in this Figure are the same as those depicted in Figure 15.

Table 2: L-panel test. Topology optimization algorithm results. \mathbf{C}^* target elasticity tensor, \mathbf{C}_{db}^h homogenized elastic tensor of the initial configuration (taken from the database), \mathbf{C}_N^h homogenized elastic tensor of the converged configuration. Values are multiplied by the factor 1000 ($E_0 = 1.MPa$). Last column displays the volume fraction of the stiff phase.

Sector		C_{1111}	C_{2222}	C_{1212}	C_{2212}	C_{1112}	C_{1122}	Vol. Frac.
1	\mathbf{C}_{db}^h	7.93	7.93	0.94	0	0	-1.79	0.30
1	\mathbf{C}_N^h	7.19	7.19	1.85	0	0	-3.12	0.17
1	\mathbf{C}^*	7.07	7.07	2.00	0	0	-3.07	-
6	\mathbf{C}_{db}^h	7.54	4.91	0.65	0	0	-1.61	0.28
6	\mathbf{C}_N^h	7.93	5.41	1.14	0	0	-2.28	0.21
6	\mathbf{C}^*	7.96	5.37	2.00	0	0	-2.27	-
13	\mathbf{C}_{db}^h	4.04	4.04	1.90	0	0	0.24	0.35
13	\mathbf{C}_N^h	4.04	4.04	2.01	0	0	0.02	0.14
13	\mathbf{C}^*	4.04	4.03	2.00	0	0	0.01	-
24	\mathbf{C}_{db}^h	13.73	3.09	1.94	0	0	-0.96	0.40
24	\mathbf{C}_N^h	13.22	4.29	1.57	0	0	-1.80	0.15
24	\mathbf{C}^*	14.03	4.35	2.00	0	0	-1.85	-
70	\mathbf{C}_{db}^h	64.21	6.72	0.09	0	0	13.79	0.12
70	\mathbf{C}_N^h	60.99	5.93	0.08	0	0	10.16	0.11
70	\mathbf{C}^*	60.75	5.90	2.00	0	0	10.14	-
72	\mathbf{C}_{db}^h	48.11	15.27	0.12	0	0	18.55	0.12
72	\mathbf{C}_N^h	47.35	13.73	0.07	0	0	20.79	0.10
72	\mathbf{C}^*	48.38	14.03	2.00	0	0	21.09	-
80	\mathbf{C}_{db}^h	82.81	2.08	2.37	0	0	-2.21	0.40
80	\mathbf{C}_N^h	80.15	3.43	0.02	0	0	-0.46	0.12
80	\mathbf{C}^*	82.43	4.00	2.00	0	0	-0.37	-
84	\mathbf{C}_{db}^h	91.52	1.64	2.20	0	0	-2.29	0.40
84	\mathbf{C}_N^h	89.69	3.19	0.02	0	0	-0.18	0.12
84	\mathbf{C}^*	91.79	4.00	2.00	0	0	-0.14	-
85	\mathbf{C}_{db}^h	93.28	5.66	0.83	0	0	2.04	0.23
85	\mathbf{C}_N^h	91.05	3.24	0.22	0	0	1.37	0.13
85	\mathbf{C}^*	91.91	4.02	2.00	0	0	0.37	-
91	\mathbf{C}_{db}^h	57.25	50.52	0.86	0	0	38.57	0.18
91	\mathbf{C}_N^h	60.84	36.03	0.76	0	0	40.68	0.17
91	\mathbf{C}^*	60.39	35.61	2.00	0	0	42.16	-

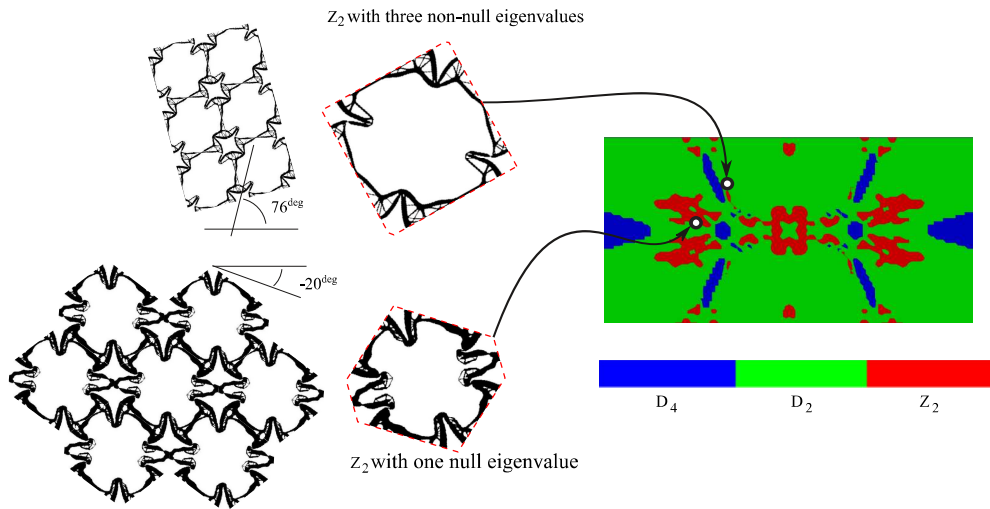


Figure 15: Computed micro-cells for two sectors of the Plate subjected to three load systems. The right picture depicts the distribution of symmetry classes. Two micro-cells are shown. The sectors with these micro-cells correspond to Z_2 symmetries with one null eigenvalue and three non-null eigenvalues, respectively.

Table 3 displays the components of the target elasticity tensor \mathbf{C}^* in the mentioned sectors. They are also compared with the homogenized elasticity tensors gathered from the database, \mathbf{C}_{db}^h , and with the homogenized elasticity tensors computed with the topology optimization algorithm \mathbf{C}_N^h .

6 Conclusions

In this paper, a two-scale material design approach, coupled in one-direction, has been explored. The effective elasticity tensors at the macro-scale are computed via a methodology based on a free parametrization of materials. Then, these effective elasticity tensors are used as target tensors for the inverse design of the micro-architectures.

This weakly coupled two-scale approach has been previously reported in the literature. However, the discussions of results obtained with it, and presented in sub-Sections 3.2, provide the necessary ingredients to state the main contributions of the paper.

These contributions focus on studying two new tools for the inverse design of material micro-architectures in optimal structural problems. They are useful procedures for attaining periodic material configurations with simple honeycomb-like micro-architectures whose effective elasticity tensors cover a wide range. The main characteristics of both tools are summarily described as follows:

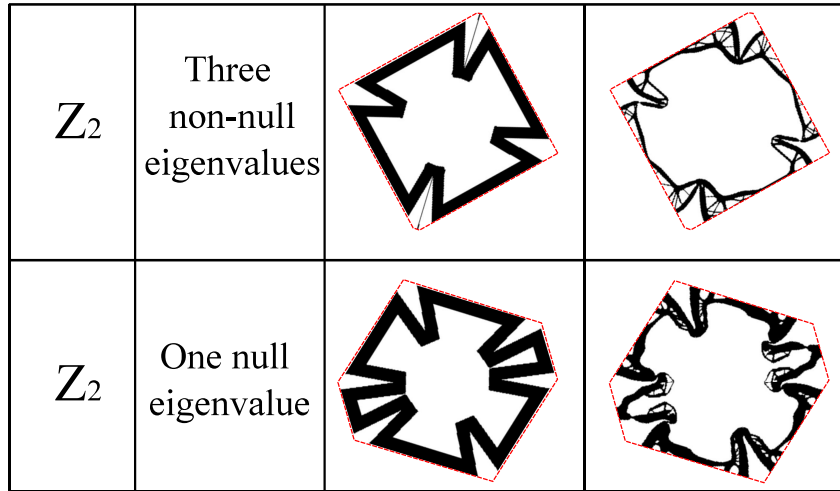


Figure 16: Plate subjected to three load systems. Configurations taken for initializing the topology optimization algorithm and the obtained solutions.

Table 3: Plate subjected to three load systems. Topology optimization algorithm results for two cases, one of them displays full anisotropic elasticity Z_2 . C^* is the target elasticity tensor, C_{db}^h is the homogenized elastic tensor of the initial configuration, gathered from the database, and C_N^h is the homogenized elastic tensor of the topology optimization algorithm converged configuration. Values are multiplied by the factor 1000 ($E_0 = 1.MPa$). Last column displays the volume fraction of the stiff phase.

Sector		C_{1111}	C_{2222}	C_{1212}	C_{2212}	C_{1112}	C_{1122}	Vol. Frac.
With one null eigenvalue	C_{db}^h	13.00	5.69	4.68	1.62	-1.62	-0.25	0.45
	C_N^h	15.52	3.56	6.72	4.13	-4.60	-2.58	0.29
	C^*	15.63	3.18	6.79	4.63	-4.63	-2.56	-
With three non-null eigenvalues	C_{db}^h	8.83	8.24	5.35	-2.17	2.17	1.94	0.35
	C_N^h	14.41	2.94	6.65	-3.46	3.68	-0.57	0.17
	C^*	14.38	2.61	6.66	-3.65	3.65	-0.63	-

- i)* The first tool defines a rule for the cell shape selection. Then, the TOP is solved in the spatial domain limited by the so-chosen cell. These cells are the Voronoi-cells of Bravais lattices having the same kind of symmetry than the one displayed by the target effective elasticity tensors.
- ii)* The other tool defines an adequate material distribution in the adopted cell. This material distribution is taken as the initial configuration for the iterative topology optimization algorithm.

An additional rule proposed in this paper is the alignment of the Voronoi-cell periodicity directions with the natural coordinate system directions of the target elasticity tensor. This rule simplifies the material distribution configurations within the Voronoi-cells. In this case, it is necessary to compute the natural coordinate system of every target elasticity tensor.

Both tools, when combined with the above-mentioned rule, mitigate the most significant limitation of the two-scale material design methodology described in this paper. This is a remarkable result which is useful for the development of realizable optimal structures using this methodology.

Finally, it is emphasized that the new proposed tools are not only limited to the inverse design of micro-architectures in the context of structural optimization problems, but also they can be applied to other more general types of metamaterial inverse homogenization problems.

Acknowledgments

The authors acknowledge the financial support from CONICET and ANPCyT (grants PIP 2013-2015 631 and PICT 2014-3372) and from the European Research Council under the European Unions Seventh Framework Programme (FP/2007-2013) / ERC Grant Agreement N. 320815 (ERC Advanced Grant Project Advanced tools for computational design of engineering materials COMP-DES-MAT).

A APPENDIX: Discretization of the FMO formulation

The finite element method is used to compute the structural response solution and evaluate $\mathbf{u} \in \mathcal{V}^{eq}$ as a function of $\hat{\mathbf{C}}(\mathbf{x})$ and \mathbf{f} . Conventional bilinear quadrilateral finite elements are used. The elasticity tensor $\hat{\mathbf{C}}_i$ is taken to be constant within every i -th finite element, with the indices: $i = 1, \dots, n_{el}$ and n_{el} is the number of finite elements in the mesh. The symmetry of each tensor $\hat{\mathbf{C}}_i$ is enforced by defining

only the six independent components, \hat{C}_{i1111} , \hat{C}_{i1122} , \hat{C}_{i1112} , \hat{C}_{i2222} , \hat{C}_{i2212} , \hat{C}_{i1212} , as design variables for the i -th finite element.

Utilizing this approach, the FMO problem can be rewritten as follows ⁷:

$$\min_{(\hat{C}_1, \dots, \hat{C}_{n_{el}}, \mathbf{u}_1, \dots, \mathbf{u}_{n_{load}})} \sum_{i=1}^{n_{el}} \text{tr}(\hat{C}_i) \Omega_i^e \quad (24a)$$

$$\text{such that: } \mathbb{K} \mathbf{u}_k - \mathbf{f}_k = \mathbf{0}; \quad \left(\mathbb{K} = \bigwedge_{j=1}^{n_{el}} \int_{\Omega_j^e} (\mathbf{B}^j)^T \hat{C}_j \mathbf{B}^j dV \right); \quad (k = 1, \dots, n_{load}) \quad (24b)$$

$$\sum_{k=1}^{n_{load}} w_k \langle \mathbf{f}_k \cdot \mathbf{u}_k \rangle \leq \bar{f}; \quad (24c)$$

$$\underline{\rho} \leq \text{tr}(\hat{C}_i) \leq \bar{\rho}; \quad (i = 1, \dots, n_{el}) \quad (24d)$$

$$\hat{C}_i \succeq 0; \quad (i = 1, \dots, n_{el}) \quad (24e)$$

where Ω_i^e is the area of the i -th finite element. Expressions (24b) are the n_{load} equilibrium equations, one for each independent load system. The stiffness matrix of the discrete equilibrium equations is denoted \mathbb{K} and is computed with a conventional numerical integration. \mathbf{B} denotes the conventional strain-displacement matrix. Expression (24e) imposes the positive semi-definite character on \hat{C}_i .

This FMO problem has $(6 \times n_{el} + n_{load} \times n_{dof})$ design variables, where n_{dof} is the number of degrees of freedom of the finite element mesh (dimension of the interpolated displacement field).

We solve the semi-definite optimization problem (24) using the IPOPT primal-dual algorithm, see Wächter and Biegler [33], with a second-order method. The Hessian matrix is simple to evaluate, but it requires enormous resources of memory. In general, problems presented in this work, up to 10000 quadrilateral finite elements, need 50 to 70 iterations. Here, we do not pursue the objective of evaluating the computational performance of IPOPT for solving very-large-scale problems. For computational benchmarks of structural optimization problems using the IPOPT algorithm, see Rojas-Labanda and Stolpe [34]. Additional information about specific algorithms designed for solving FMO problems can be found in the paper of Weldeyesus and Stolpe [9] and references cited therein.

⁷Introducing an abuse of notation, discrete and continuous fields in this Section are identified with the same symbols.

B APPENDIX: Symmetries of the elasticity tensor in plane problems

Let us consider a generic plane elasticity tensor \mathbf{C} . In the Cartesian coordinate system, its components are denoted C_{ijkl} , with $i, j, k, l = 1, 2$.

Following the Kelvin's notation, this tensor can be written in the matrix format

$$\mathbf{C} = \begin{bmatrix} C_{1111} & C_{1122} & \sqrt{2}C_{1112} \\ C_{2211} & C_{2222} & \sqrt{2}C_{2212} \\ \sqrt{2}C_{1211} & \sqrt{2}C_{1222} & 2C_{1212} \end{bmatrix}. \quad (25)$$

Also, \mathbf{C} can be expressed in the normal coordinate system (normal basis), see Aufferay and Ropars [35] and Cowin and Mehrabadi [36]. The normal coordinate system is rotated an angle θ respect to the Cartesian coordinate system.

In normal coordinates, the tensor (25) is represented by the matrix

$$\mathbf{C}_N = \begin{bmatrix} K + G + a_1 + d_1 & K - G - d_1 & \sqrt{2}d_2 \\ K - G - d_1 & K + G - a_1 + d_1 & -\sqrt{2}d_2 \\ \sqrt{2}d_2 & -\sqrt{2}d_2 & 2G - 2d_1 \end{bmatrix}, \quad (26)$$

called the normal form of \mathbf{C} . In this expression, K , G , a_1 , d_1 and d_2 are material parameters. The angle θ should also be considered as an additional material parameter. Note that θ is the rotation angle taking the matrix (25) and transforming it to expression (26).

According to the symmetry group qualifying \mathbf{C}_N , these material parameters K , G , a_1 , d_1 and d_2 are:

- Symmetry Z_2 (anisotropic) has six independent elastic coefficients: K , G , a_1 , d_1 and d_2 plus the angle θ . The normal form of \mathbf{C}_N results with the components $(C_N)_{1112} = -(C_N)_{2212}$.
- Symmetry D_2 (orthotropic) has five independent elastic coefficients: K , G , a_1 and d_1 plus the angle θ . The normal form of \mathbf{C}_N results with the components $(C_N)_{1112} = (C_N)_{2212} = 0$ ($d_2 = 0$).
- Symmetry D_4 (tetragonal) has four independent elastic coefficients: K , G and d_1 plus the angle θ that should be defined such that $a_1 = d_2 = 0$. The normal form of \mathbf{C}_N results with the components: $(C_N)_{1111} = (C_N)_{2222}$ and $(C_N)_{1112} = (C_N)_{2212} = 0$.
- Symmetry $O(2)$ (isotropic), has two independent elastic coefficients: K , G . The angle θ is arbitrary. Then, The normal form of \mathbf{C}_N results with the

components: $(C_N)_{1111} = (C_N)_{2222}$, $(C_N)_{1212} = (C_N)_{1111} - (C_N)_{1122}$ and $(C_N)_{1112} = (C_N)_{2212} = 0$. In this particular case, we identify

$$\kappa = K - \frac{G}{3}, \quad (27)$$

where, κ is the 3-D bulk modulus and G is the shear modulus.

In all cases, except for isotropic symmetry, the angle θ is an additional parameter of the elasticity tensor.

We recall that the normal format (26) of \mathbf{C} is not preserved in arbitrary Cartesian bases.

B.1 Reorientation of the elasticity tensor to the normal basis

The rotation angle θ transforming \mathbf{C} to the normal axis is found with the algorithm proposed by Auffray and Ropars [35], see also [37].

Auffray et al. introduce the fourth and second order tensors denoted \mathbf{D} , \mathbf{a} and the coefficients λ and μ . All these terms are defined as follows:

$$\begin{aligned} D_{ijkl} &= C_{ijkl} - \\ &\quad - \frac{1}{6}(\delta_{ij}C_{kplp} + \delta_{kl}C_{ipjp} + \delta_{ik}C_{lpjp} + \delta_{lj}C_{ipkp} + \delta_{il}C_{jpkp} + \delta_{jk}C_{iplp}) \\ &\quad + \frac{C_{ppqq}}{12}(5\delta_{ij}\delta_{kl} - \delta_{ik}\delta_{jl} - \delta_{il}\delta_{jk}) - \frac{C_{ppqq}}{8}(3\delta_{ij}\delta_{kl} - \delta_{ik}\delta_{jl} - \delta_{il}\delta_{jk}), \quad (28) \\ a_{ij} &= \frac{1}{12}(2C_{ipjp} - C_{ppqq}\delta_{ij}), \\ \lambda &= \frac{1}{8}(3C_{ppqq} - 2C_{ppqq}), \\ \mu &= \frac{1}{8}(2C_{ppqq} - C_{ppqq}). \end{aligned}$$

With these expressions, the invariants of \mathbf{C} are calculated

$$\begin{aligned} I_1 &= \lambda + \mu, & J_1 &= \mu, & I_2 &= a_{pq}a_{pq}, \\ J_2 &= D_{pqrs}D_{pqrs}, & I_3 &= a_{pq}D_{pqrs}a_{rs}, & J_3 &= R_{pq}a_{qr}D_{prst}a_{st}. \end{aligned} \quad (29)$$

where the tensor:

$$R = \begin{pmatrix} 0 & 1 \\ -1 & 0 \end{pmatrix},$$

These invariants define the symmetry class of \mathbf{C} . The procedure is described in Figure 17. Also, the coefficient determining the normal form of \mathbf{C} , equation (26), are determined with expressions (28) as follows:

$$\begin{aligned}
K &= I_1, \\
G &= J_1, \\
a_1 &= \frac{1}{2}(a_{11} - a_{22}) , \\
a_2 &= \frac{1}{2}(a_{12} + a_{21}) , \\
d_1 &= \frac{\sqrt{8}}{8}(D_{1111} + D_{2222} - D_{1122} - D_{1212} \\
&\quad - D_{2112} - D_{2121} - D_{1221} - D_{2211}) , \\
d_2 &= \frac{\sqrt{8}}{8}(D_{1112} + D_{1121} + D_{1211} + D_{2111} \\
&\quad - D_{2221} - D_{2212} - D_{2122} - D_{1222}) ,
\end{aligned}$$

Also, defining the angles:

$$\theta_\alpha = \frac{1}{2} \tan^{-1} \left(\frac{a_2}{a_1} \right) \quad ; \quad \theta_\beta = \frac{1}{4} \tan^{-1} \left(\frac{d_2}{d_1} \right) ,$$

the angle θ is determined with the rule: $\theta = \theta_\alpha$ for the classes Z_2 or D_2 ; and $\theta = \theta_\beta$ for the class D_4 .

References

- [1] M.P. Bendsøe, J.M. Guedes, R.B. Haber, P. Pedersen, and J.E. Taylor. An analytical model to predict optimal material properties in the context of optimal structural design. *Journal of Applied Mechanics*, 61(4):930–937, 1994.
- [2] M.P. Bendsøe, A.R. Díaz, R. Lipton, and J.E. Taylor. Optimal design of material properties and material distribution for multiple loading conditions. *International Journal for Numerical Methods in Engineering*, 38(7):1149–1170, 1995.
- [3] U.T. Ringertz. On finding the optimal distribution of material properties. *Structural and Multidisciplinary Optimization*, 5(4):265–267, 1993.
- [4] M.P. Bendsøe. Optimization of structural topology, shape, and material, 1995.
- [5] M.P. Bendsoe and O. Sigmund. *Topology optimization: theory, methods, and applications*. Springer, Berlin., 2003.

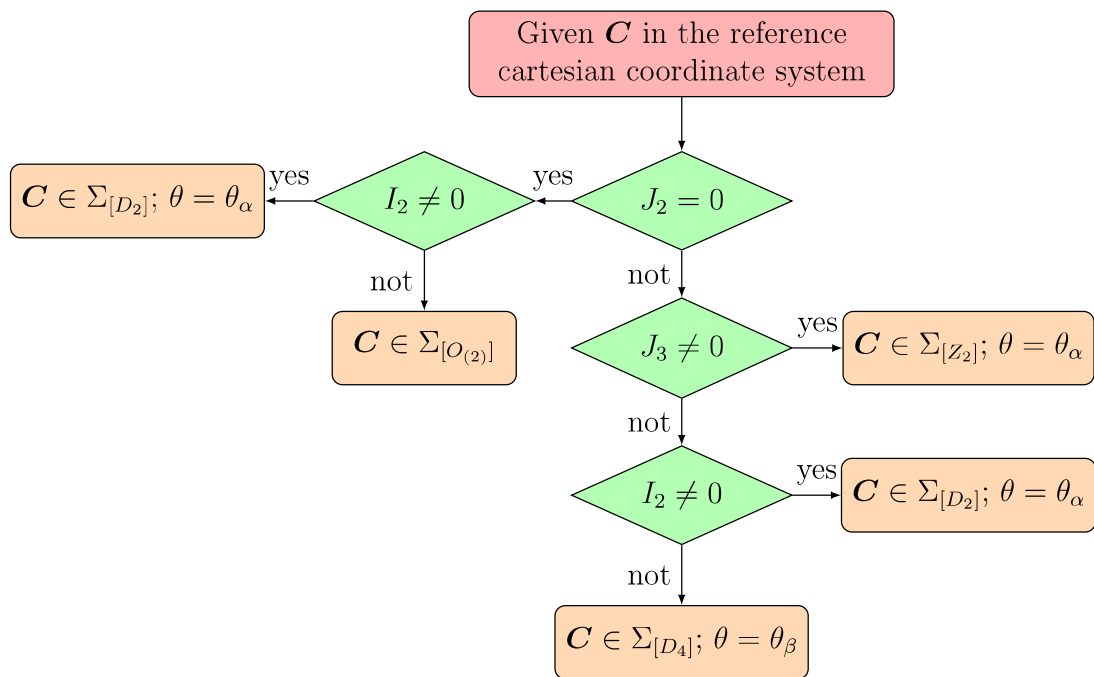


Figure 17: Classification of \mathbf{C} -symmetry and angle θ between the normal basis and the Cartesian basis (Auffray and Ropars [35])

- [6] J. Zowe, M. Kočvara, and M.P. Bendsøe. Free material optimization via mathematical programming. *Mathematical programming*, 79(1):445–466, 1997.
- [7] M. Kočvara, M. Stingl, and J. Zowe. Free material optimization: recent progress. *Optimization*, 57(1):79–100, 2008.
- [8] M. Stingl, M. Kočvara, and G. Leugering. A sequential convex semidefinite programming algorithm with an application to multiple-load free material optimization. *SIAM Journal on Optimization*, 20(1):130–155, 2009.
- [9] A.G. Weldeyesus and M. Stolpe. A primal-dual interior point method for large-scale free material optimization. *Computational Optimization and Applications*, 61(2):409–435, 2015.
- [10] O. Sigmund. Materials with prescribed constitutive parameters: an inverse homogenization problem. *International Journal of Solids and Structures*, 31(17):2313–2329, 1994.
- [11] O. Sigmund. A new class of extremal composites. *Journal of the Mechanics and Physics of Solids*, 48(2):397–428, 2000.
- [12] F. Schury, M. Stingl, and F. Wein. Efficient two-scale optimization of manufacturable graded structures. *SIAM Journal on Scientific Computing*, 34(6):B711–B733, 2012.
- [13] G. Allaire. *Shape optimization by the homogenization method*, volume 146. Springer Science & Business Media, 2012.
- [14] A. Cherkaev. *Variational methods for structural optimization*, volume 140. Springer Science & Business Media, 2012.
- [15] G.W. Milton and A.V. Cherkaev. Which elasticity tensors are realizable? *Journal of engineering materials and technology*, 117(4):483–493, 1995.
- [16] F. Schury. Two-scale material design-from theory to practice. 2013. PhD Thesis, Friedrich-Alexander-Universität Erlangen-Nürnberg.
- [17] S. Amstutz and H. Andrä. A new algorithm for topology optimization using a level-set method. *Journal of Computational Physics*, 216(2):573–588, 2006.
- [18] S. Amstutz, S.M. Giusti, A.A. Novotny, and E.A. de Souza Neto. Topological derivative for multi-scale linear elasticity models applied to the synthesis of microstructures. *International Journal for Numerical Methods in Engineering*, 84(6):733–756, 2010.

- [19] A.R. Diaz and A. Benard. Designing materials with prescribed elastic properties using polygonal cells. *International Journal for Numerical Methods in Engineering*, 57(3):301–314, 2003.
- [20] S.M. Giusti, A. Ferrer, and J. Oliver. Topological sensitivity analysis in heterogeneous anisotropic elasticity problem. theoretical and computational aspects. *Computer Methods in Applied Mechanics and Engineering*, 311:134–150, 2016.
- [21] G.W. Milton. The theory of composites. *The Theory of Composites, by Graeme W. Milton, pp. 748. ISBN 0521781256. Cambridge, UK: Cambridge University Press, May 2002.*, page 748, 2002.
- [22] T.C. Ting. *Anisotropic elasticity: theory and applications*. Number 45. Oxford University Press, 1996.
- [23] P. Pedersen. On optimal orientation of orthotropic materials. *Structural and Multidisciplinary Optimization*, 1(2):101–106, 1989.
- [24] O. Sigmund. Design of material structures using topology optimization. 1994. PhD thesis, Technical University of Denmark.
- [25] C.G. Lopes, R.B. dos Santos, and A.A. Novotny. Topological derivative-based topology optimization of structures subject to multiple load-cases. *Latin American Journal of Solids and Structures*, 12(5):834–860, 2015.
- [26] C. Méndez, J.M. Podestá, O. Lloberas-Valls, S. Toro, A.E. Huespe, and J. Oliver. Computational material design for acoustic cloaking. *International Journal for Numerical Methods in Engineering*, 2017.
- [27] S. Amstutz. Analysis of a level set method for topology optimization. *Optimization Methods and Software*, 26(4-5):555–573, 2011.
- [28] N.W. Ashcroft and N.D. Mermin. *Solid State Physics*. Harcourt College Publishers, New York), 1976.
- [29] C. Kittel. Introduction to solid state physics. *University of Pennsylvania Law Review*, 154(3):477, 2005.
- [30] C. Méndez, J.M. Podestá, S. Toro, A.E. Huespe, and J. Oliver. In preparation, 2017.
- [31] H. M.A. Kolken and A.A. Zadpoor. Auxetic mechanical metamaterials. *RSC Advances*, 7(9):5111–5129, 2017.

- [32] M.H. Fu, O.T. Xu, L.L. Hu, and T.X. Yu. Nonlinear shear modulus of re-entrant hexagonal honeycombs under large deformation. *International Journal of Solids and Structures*, 80:284–296, 2016.
- [33] A. Wächter and L.T. Biegler. On the implementation of a primal-dual interior point filter line search algorithm for large-scale nonlinear programming. *Mathematical Programming*, 106(1):25–57, 2006.
- [34] S. Rojas-Labanda and M. Stolpe. Benchmarking optimization solvers for structural topology optimization. *Structural and Multidisciplinary Optimization*, 52(3):527–547, 2015.
- [35] N. Auffray and P. Ropars. Invariant-based reconstruction of bidimensional elasticity tensors. *International Journal of Solids and Structures*, 87:183–193, 2016.
- [36] S.C. Cowin and M.M. Mehrabadi. On the identification of material symmetry for anisotropic elastic materials. *Quarterly Journal of Mechanics and Applied Mathematics*, 40(Part 4):451–476, 1987.
- [37] M. Vianello. An integrity basis for plane elasticity tensors. *Archives of Mechanics*, 49(1):197–208, 1997.